



Mössbauer spectroscopy study of Y-type Hexaferrite ($\text{Ba}_2\text{Co}_2\text{Fe}_{12}\text{O}_{22}$) prepared by the co-precipitation method

Abdel-Fatah Lehlooh¹  · Reham Alghazo¹ · Fuad Rawwagah¹ · Ayman Hammoudeh² · Sami Mahmood³

Published online: 17 December 2019
© Springer Nature Switzerland AG 2019

Abstract

In this work we report the results of structural and Mössbauer spectroscopy studies for $\text{Ba}_2\text{Co}_2\text{Fe}_{12}\text{O}_{22}$ samples prepared by coprecipitation following two different synthesis routes: route A (pH = 10, NaOH + Na_2CO_3 added dropwise), and route B (pH = 14, NaOH + Na_2CO_3 added one shot). The resulting powders were sintered for 4 h at different temperatures (700 °C to 1100 °C in steps of 100 °C). The sintered powders were characterized by x-ray diffraction (XRD) and room temperature Mössbauer spectroscopy. XRD and Mössbauer results of the sample prepared by route A and sintered at 700 °C revealed formation of spinel phases (CoFe_2O_4 and/or Fe_3O_4), BaCO_3 and BaM-type phase. The Co_2Y phase developed in the samples sintered at 800 °C and 900 °C with spinel species as impurities, and single (pure) Co_2Y phase was obtained at higher temperatures. On contrast, XRD patterns and the Mössbauer spectra for the samples prepared by route B showed different results, where the sample sintered at 700 °C consisted of only spinel phases. The Co_2Y phase developed at higher temperatures, coexisting with significant amounts of other phases.

Keywords $\text{Ba}_2\text{Co}_2\text{Fe}_{12}\text{O}_{22}$ · Y-type hexaferrite · X-ray diffraction · Coprecipitation · Mössbauer spectroscopy · Sintering

This article is part of the Topical Collection on *Proceedings of the International Conference on the Applications of the Mössbauer Effect (ICAME2019)*, 1-6 September 2019, Dalian, China
Edited by Tao Zhang, Junhu Wang and Xiaodong Wang

✉ Abdel-Fatah Lehlooh
aflehlooh@yu.edu.jo

¹ Department of Physics, Yarmouk University, Irbid, Jordan

² Department of Chemistry, Yarmouk University, Irbid, Jordan

³ Department of Physics, The University of Jordan, Amman, Jordan

1 Introduction

Ferrites, consisting of iron oxide as their main constituent, belong to an important class of magnetic materials which have been extensively synthesized and characterized due to their importance in the technological and industrial sectors [1–7]. Interest in ferrites as technologically important materials developed as a consequence of several parameters: they are cost effective, chemically stable, and easily synthesized with a wide range of magnetic properties covering the requirements for a wide range of applications. Their applications include transformer cores, multilayer chip inductors, high quality filters, passive components of high frequency devices, permanent magnets, magnetic recording, and many more. Hexagonal ferrites constitute an important class of the ferrite family, which demonstrated superior properties to other types of ferrites in permanent magnet [6, 8, 9], magnetic recording [10, 11], multiferroics [12–14], and microwave applications [15–17].

Hexaferrites are classified according to their structure into six main types, namely, M-type ($\text{BaFe}_{12}\text{O}_{19}$), Y-type ($\text{Ba}_2\text{Me}_2\text{Fe}_{12}\text{O}_{22}$), W-type ($\text{BaMe}_2\text{Fe}_{16}\text{O}_{27}$), X-type ($\text{Ba}_2\text{Me}_2\text{Fe}_{28}\text{O}_{46}$), Z-type ($\text{Ba}_3\text{Me}_2\text{Fe}_{24}\text{O}_{41}$), and U-type ($\text{Ba}_4\text{Me}_2\text{Fe}_{36}\text{O}_{60}$), where Me represents a divalent metal ion (Co^{2+} , Zn^{2+} , Ni^{2+} , Mg^{2+} , etc.). Extensive research work revealed that the properties of hexagonal ferrites may depend critically on the synthesis route and experimental conditions. Accordingly, several articles and reviews concerning the influence of the synthesis route and experimental conditions on the structural and magnetic properties of hexagonal ferrites were recently published [3, 18–24]. Also, the properties of the hexaferrites were modified by substitution of Ba^{2+} ions by another large ion such as Sr^{2+} [25–28], or Pb^{2+} [29, 30], and by changing the Me ion, and/or partial substitution for Fe^{3+} ions [31–39].

All hexaferrite unit cells are composed of sub-structural blocks (S, R and T). The S block is formed by two formula units of Fe_3O_4 with the spinel structure containing two tetrahedral and four octahedral cation sites. The T block has four layers with the formula $\text{Ba}_2\text{Fe}_8\text{O}_{14}$, where Fe ions occupy two tetrahedral sites, and six octahedral sites of two distinct types. The R block has stoichiometry $\text{BaFe}_6\text{O}_{11}$ with five octahedral sites of different types and one trigonal bipyramidal site [40].

The crystalline structure of Y-type $\text{A}_2\text{Me}_2\text{Fe}_{12}\text{O}_{22}$, where A represents an alkaline-earth element (i.e. Ba and Sr), consists of blocks STS??T??S"?"T"; the (??) denotes a rotation by 120° about hexagonal axis. The space group of Y type structure is R3m, with hexagonal parameters: $a = 5.9 \text{ \AA}$ and $c = 43.56 \text{ \AA}$. The metallic cations (Me and Fe^{3+}) are distributed among six sublattices, two tetrahedral sites ($6c_{IV}$ and $6c_{IV}^*$) and four octahedral sites ($3a_{VI}$, $3b_{VI}$, $6c_{VI}$, and $18h_{VI}$), as indicated in Table 1.

Y-type hexagonal hexaferrites have gained interest in recent years due to their multiferroic properties [41, 42]. With special experimental design, Y-type hexaferrite can be synthesized at lower temperature than other hexaferrites, which is a requirement for device design [43]. In

Table 1 Metallic sublattices of Y structures and their properties

Sublattices	Coordination	Block	Number of ions per unit cell	Spin
$6c_{IV}$	Tetra	S	6	Down
$3a_{VI}$	Octa	S	3	Up
$18h_{VI}$	Octa	S-T	18	Up
$6c_{VI}$	Octa	T	6	Down
$6c_{IV}^*$	Tetra	T	6	Down
$3b_{VI}$	Octa	T	3	Up

this study we employed the coprecipitation method to prepare samples of barium Co_2Y hexaferrite ($\text{Ba}_2\text{Co}_2\text{Fe}_{12}\text{O}_{22}$) using two different synthesis routes. The samples were characterized by XRD, and hyperfine interactions were investigated by Mössbauer Spectroscopy to monitor the sites occupancy of the metal ions in the different sublattices of the ferrite structure.

2 Experimental

2.1 System preparation

In this work we prepared different ferrite systems by applying the coprecipitation method. Using this technique, stoichiometric precursor mixtures of soluble salts of the metals were prepared, and mixed to form a homogeneous solution. Then the mixture was precipitated as hydroxides, citrates, oxalates, or formates. Afterward the mixture was filtered, dried, and then heated to give the final product. Different parameters and conditions of coprecipitation processes can influence the final product significantly. These include precipitant concentration and addition methods, pH, temperature, mixing method and time, temperature and time of drying and calcination [44]. In the following we describe the procedures we followed to control the precipitation process:

- Procedure A: pH = 10, coprecipitation with NaOH and Na_2CO_3 , dripping

Stoichiometric amount of $\text{Ba}_2(\text{NO}_3)_2$, $\text{Co}(\text{NO}_3)_2 \cdot 6\text{H}_2\text{O}$, and $\text{Fe}(\text{NO}_3)_3 \cdot 9\text{H}_2\text{O}$ were dissolved in 500 ml of distilled water. The precipitant solution was prepared by dissolving 14.14 g of Na_2CO_3 and 5.11 g of NaOH in 200 ml of distilled water. The precipitant was added slowly in the stoichiometric mixture to adjust the pH level to 10. The resulting mixture was stirred for one hour at room temperature. After precipitation is accomplished, the precipitate was filtered and washed thoroughly with deionized water three times. Then, the precipitate was dried for 10 h at 100 °C and ground into powder form. Portions of this powder were pressed in pellets (circular disks) and then sintered at different temperatures (700 °C to 1100 °C in steps of 100 °C) for 4 h with heating rate of 10 °C/min using an open tube furnace. The hexaferrite powder samples produced were labeled as A-700, A-800, A-900, A-1000, and A-1100. The letter and the number indicate preparation procedure and sintering temperature, respectively.

- Procedure B: pH = 14, coprecipitation with NaOH and Na_2CO_3 , one shot

Stoichiometric amount of $\text{Ba}_2(\text{NO}_3)_2$, $\text{Co}(\text{NO}_3)_2 \cdot 6\text{H}_2\text{O}$, and $\text{Fe}(\text{NO}_3)_3 \cdot 9\text{H}_2\text{O}$ were dissolved in 500 ml of distilled water. The precipitant solution was prepared by dissolving 12.05 g of Na_2CO_3 and 10.05 g of NaOH in 200 ml of distilled water. The precipitant was added one shot in the stoichiometric mixture to adjust the pH level to 14. The resulting mixture was stirred for one hour at room temperature. After precipitation is accomplished, the coprecipitated powders were filtered and washed thoroughly with deionized water three times. Then, the precipitate was dried for 6 h at 100 °C and ground into powder form. Portions of this powder were pressed in pellets (circular disks) and then sintered at different temperatures (700 °C to 1100 °C in steps of 100 °C) for 4 h with heating rate of 10 °C/min using an open tube furnace. The hexaferrite powder samples produced were labeled as B-700, B-800, B-900, B-1000, and B-1100.

2.2 Mössbauer spectroscopy

Mössbauer samples were prepared as a thin circular layer of the system powder pressed gently between two Teflon disks. The Mössbauer spectra were collected using standard constant acceleration Mössbauer spectrometer over 1024 channels with a ^{57}Co Mössbauer source. The Mössbauer spectra are analyzed using standard fitting routines to obtain the hyperfine parameters.

The spectrum of α -Iron was used to calibrate the system. The standard value for the hyperfine field of ^{57}Fe is 33.0 T.

2.3 X-ray diffraction (XRD)

The X-ray diffraction patterns of the prepared system were recorded using a $(\theta-2\theta)$ -shimadzu-diffractometer. $\text{Cu}-\text{K}\alpha$ radiation, with weighted average wavelength for $\text{K}\alpha_1$ and $\text{K}\alpha_2$ $\lambda = 1.5406 \text{ \AA}$, was used. The diffraction patterns were recorded over the angular range of $20^\circ < 2\theta < 80^\circ$. The XRD patterns were analyzed to figure out the phases formed during the stages of preparation and the average particles size of the resulting systems.

3 Results and discussion

We will discuss the results of the X-ray diffraction (XRD) and Mössbauer spectroscopy (MS) measurements of the Y-type hexaferrite powder $\text{Ba}_2\text{Co}_2\text{Fe}_{12}\text{O}_{22}$ that were prepared by the Coprecipitation method with different preparation conditions and sintering temperatures.

3.1 XRD measurements

- $\text{Ba}_2\text{Co}_2\text{Fe}_{12}\text{O}_{22}$ (A, 700°C to 1100°C)

Figure 1 shows the XRD patterns for the samples A-700, A-800, A-900, A-1000 and A-1100. These samples were prepared using procedure A and sintered at the temperatures indicated by their labels (700 °C to 1100 °C). The XRD pattern for the sample A-700 shows no Bragg reflections of the Co_2Y phase but reflections corresponding to other oxide species: BaM-type hexaferrite phase, BaCO_3 and the spinels (CoFe_2O_4 or/and Fe_3O_4). These phases are intermediate phases for the Co_2Y phase [45]. The XRD patterns for the samples A-800 and A-900 show Bragg peaks corresponding to Co_2Y phase when compared with the standard pattern of this phase (JCPDS 00–044–0206) and tiny traces of Ba-spinel (BaFe_2O_4) phase, which is characterized by the very small peak at $\theta \cong 28.3^\circ$. When compared with the standard (JCPDS 00–044–0206), the XRD patterns for the samples A-1000 and A-1100 show peaks corresponding totally to pure Co_2Y phase. These results indicated that through procedure A, we achieved the Co_2Y phase with relatively high purity at a relatively low temperature of 800 °C (only small amounts of Ba-spinel impurity was observed). However, pure Co_2Y phase was achieved by sintering at 1000 °C and 1100 °C.

Rietveld refinement of the patterns corresponding to the samples (A-800 to A-1100) was performed using fullProf and shown in Fig. 2. Rietveld analysis of the patterns revealed that both A-1100 and A-1000 are single Co_2Y phase while the A-900 and A-800 have around 2% of Ba-spinel species in addition to the main Co_2Y phase.

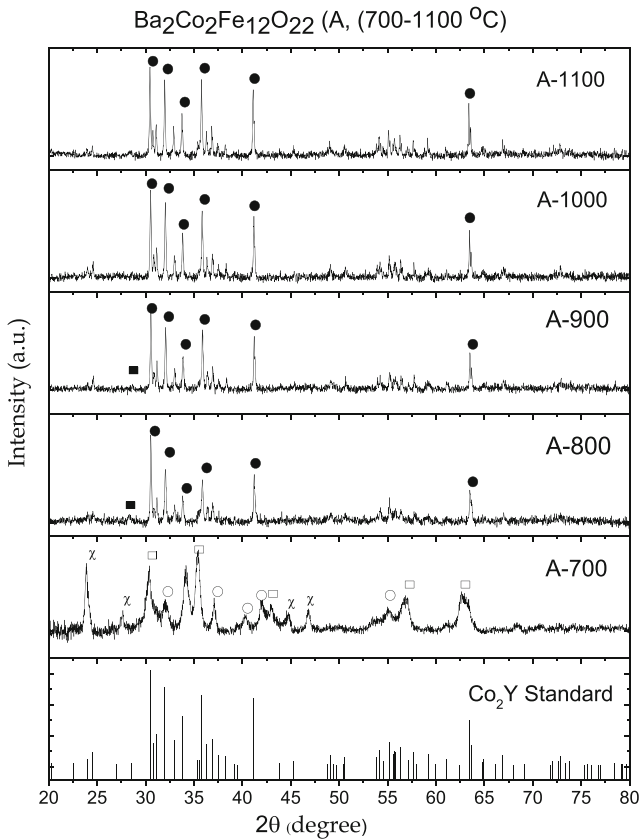


Fig. 1 XRD patterns for the samples prepared using procedure A and sintered at different temperatures (700 °C to 1100 °C): (A-700, A-800, A-900, A-1000, A-1100) with symbols denoting phases, where closed circles denote Y-type hexaferrite peaks, open circles denote M-type peaks, open squares denote $(\text{CoFe}_2\text{O}_4$ and/or $\text{Fe}_3\text{O}_4)$, closed squares denote $(\text{BaFe}_2\text{O}_4)$ and χ denote (BaCO_3)

• $\text{Ba}_2\text{Co}_2\text{Fe}_{12}\text{O}_{22}(\text{B}, 700\text{ }^\circ\text{C to } 1100\text{ }^\circ\text{C})$

The XRD patterns for the samples prepared by procedure B and sintered at temperatures (700 °C to 1100 °C) (named B-700, B-800, B-900, B-1000 and B-1100) are shown in Fig. 3. The XRD patterns show complicated structure where each pattern has its own distinguished structure. The XRD pattern for the sample B-700 shows no traces of the Co_2Y phase but Ba-spinel (BaFe_2O_4) and other spinels (CoFe_2O_4 and/or Fe_3O_4) as main phases. The presence of a small peak at $\theta \cong 24^\circ$ is attributed to the major peak for BaCO_3 structure (JCPDS 00-044-1487). This indicates that traces of BaCO_3 are still present in the sample.

The XRD pattern for the sample B-800 shows the presence of Co_2Y hexaferrite phase ($\text{Ba}_2\text{Co}_2\text{Fe}_{12}\text{O}_{22}$) as a main phase, and around 4% of BaFe_2O_4 and cubic spinel phases.

The XRD patterns for the samples B-900 and B-1000 show the presence of both Co_2Y hexaferrite ($\text{Ba}_2\text{Co}_2\text{Fe}_{12}\text{O}_{22}$) and Ba-spinel (BaFe_2O_4). Tiny traces (around 2.5%) of other spinels (CoFe_2O_4 and/or Fe_3O_4) are detected too in the XRD patterns for both samples.

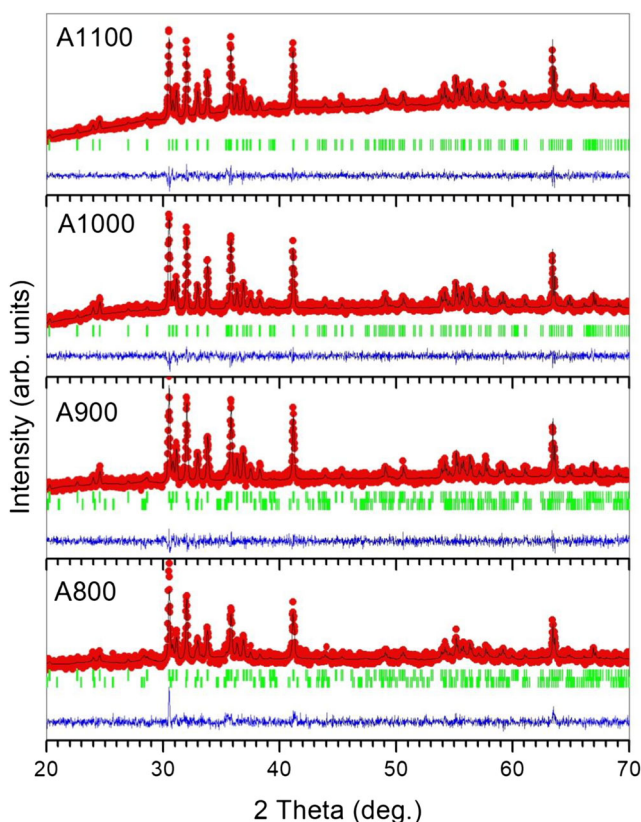


Fig. 2 Rietveld refinement of XRD patterns for the A-800 to A-1100 samples

The XRD pattern for the sample B-1100 shows the presence of Co_2Y phase ($\text{Ba}_2\text{Co}_2\text{Fe}_{12}\text{O}_{22}$) as a main phase and around 5% of spinel (CoFe_2O_4 and/or Fe_3O_4) phase. In fact, this result was unexpected as the BaM-type phase is a precursor and is supposed to appear as an intermediate stage for the Co_2Y phase formation [45]. This is an indication that the reaction kinetics and product was significantly altered by the imposed change in experimental procedure. In a recent study, it was demonstrated that the pH value and the sintering temperature play an important role in modifying the structural and magnetic properties of spinel ferrites [46]. The reported estimations of the minor phases are revealed from the Rietveld refinement analysis of the patterns for the B-800 to B-1100 samples. Its Rietveld refinement spectra are shown in Fig. 4.

3.1.1 Average crystallite sizes

The average crystallite size for the Co_2Y phase in all samples was calculated using Scherrer formula [47]: $D = K\lambda/\beta \cos \theta$, where D is the crystallite size, K is the Scherrer constant (0.94), ($\lambda = 1.5406 \text{ \AA}$) is the x-ray wavelength, β is the peak width at half maximum measured in radians, and θ is the peak position. The calculated average crystallite sizes are tabulated in Table 2.

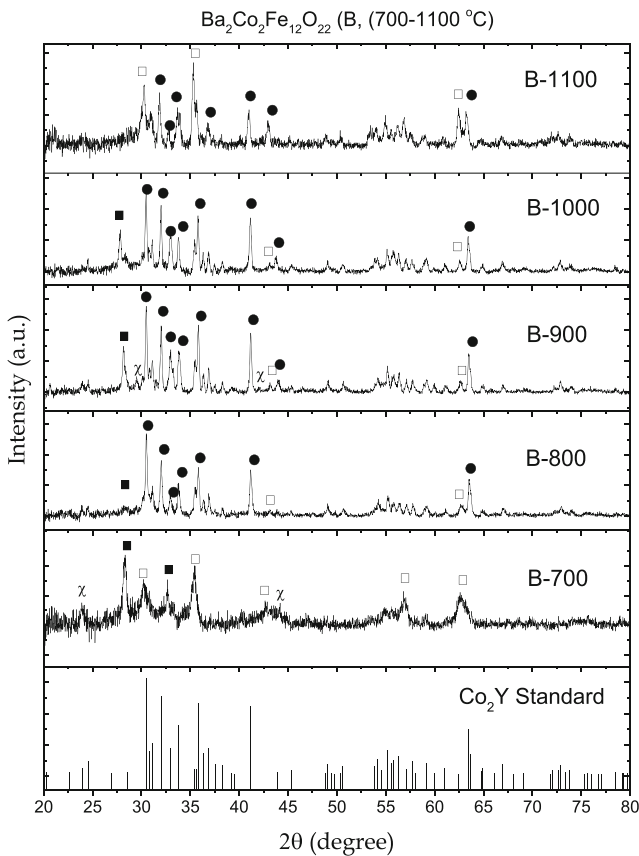


Fig. 3 XRD patterns for the samples prepared using procedure B and sintered at different temperatures (700 °C to 1100 °C): (B-700, B-800, B-900, B-1000, B-1100) with symbols denoting phases, where closed circles denote Y-type hexaferrite peaks, open squares denote (CoFe₂O₄ and/or Fe₃O₄), closed squares denote (BaFe₂O₄) and χ denote (BaCO₃)

3.2 Mössbauer spectroscopy

Room temperature Mössbauer spectra were recorded for all samples of the systems Ba₂Co₂Fe₁₂O₂₂. The spectra were each fitted with the appropriate type and number of components.

- Ba₂Co₂Fe₁₂O₂₂ (A, 700 °C to 1100 °C) Samples

The Mössbauer spectra for the samples A-700, A-800, A-900, A-1000, A-1100 prepared by procedure A and sintered at 700, 800, 900, 1000, 1100 °C, respectively, are shown in Fig. 5. The figure shows similar spectral structure for the samples A-800, A-900, A-1000, A-1100 and significantly different spectral characteristics for the sample A-700. This is consistent with XRD findings, which revealed that the samples sintered at temperatures ≥ 800 °C all consisted of a major Co₂Y hexaferrite phase, whereas the sample sintered at 700 °C consisted of other phases. The Mössbauer spectra of all samples except A-700 show broad hyperfine splitting.

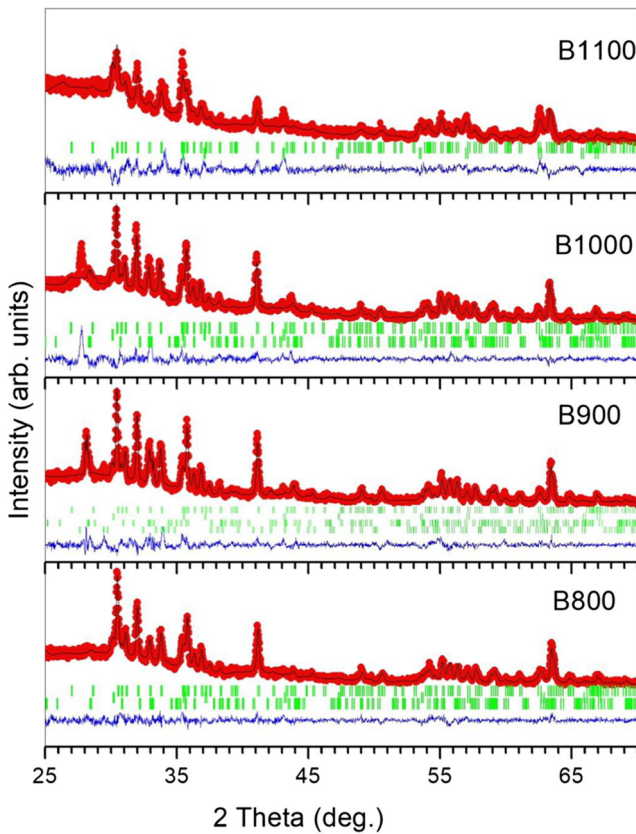


Fig. 4 Rietveld refinement of XRD patterns for the B-800 to B-1100 samples

Hence, they were fitted with three magnetic components (sextets), as it was difficult to fit them with six components associated with the six iron sites ($6c_{VI}$, $6c_{IV}$, $3a_{VI}$, $6c_{IV}^*$, $3b_{VI}$, $18h_{VI}$) in the Co_2Y hexaferrites, due to similarity of the hyperfine parameters of certain sets of sites. Throughout the fitting procedure and interpretation of the sub-spectral components, we followed Mahmood et al. [31]. The high field component (I) is associated with the ($6c_{IV}^* + 3b_{VI}$) sites. The maximum capacity of these sites is 3 ions, leading to maximum relative intensity of 25%. The middle component (II) is associated with the $18h_{VI}$ sites. The maximum capacity of these sites is 6 ions, leading to maximum relative intensity of 50%. The low field component (III) is associated with the ($6c_{VI} + 6c_{IV} + 3a_{VI}$) sites. The maximum capacity of these sites is 5 ions, leading to maximum relative intensity of 41.6%. The fitting parameters for the spectra of all samples are listed in Table 3. The observed relative intensity of 25% for component III (Table 3) is an indication that the corresponding sites are occupied by 3 Fe^{+3} ions and 2 Co^{+2} ions. Accordingly, we may conclude that Co^{+2} ions occupy the $6c_{VI}$ sites. This

Table 2 The average crystallites sizes for the $Ba_2Co_2Fe_{12}O_{22}$ phase in all the samples

Sample	A-800	A-900	A-1000	A-1100	B-800	B-900	B-1000
D(nm) (± 5)	65	69	70	86	49	53	50

is in light of the fact that ions with lower valence states should occupy face-sharing polyhedra in order to reduce the electrostatic energy of the crystal [31, 40]. The relative intensities of the three sextet components (I,II,III) for the spectra with high sintering temperatures were fixed to be (1:2:1). Due to symmetry of the spectra, the quadrupole splitting was ignored in the fitting procedure.

Mössbauer spectrum for the A-700 sample was fitted with four magnetic sextets (with quadrupole shifts) and one pure quadrupole component (doublet), and the Mössbauer fitting parameters are listed in Table 3. The values of hyperfine fields were found to be $B_{\text{hf}} = 50.9$ T, 47.8 T, 41.6 T and 39.0 T and the corresponding quadrupole shifts are: $QS = 0.17, 0.21, 0.47$ and 0.13 mm/s. These four magnetic sextets are associated with the four major iron sites in the BaM hexaferrite structure. The obtained values of the Mössbauer parameters agree with those

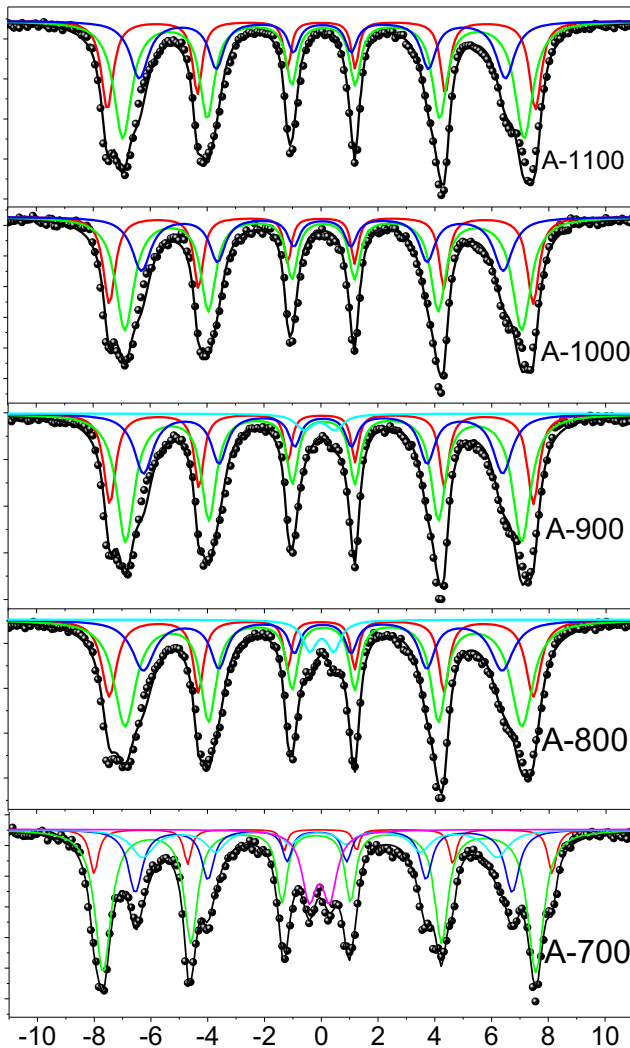


Fig. 5 Mössbauer spectra for the $\text{Ba}_2\text{Co}_2\text{Fe}_{12}\text{O}_{22}$ samples (A-700, A-800, A-900, A-1000 and A-1100) prepared using procedure A and sintered at different temperatures (700 °C to 1100 °C)

Table 3 Mössbauer parameters of the spectral components for samples prepared by procedure A and sintered at different temperatures (700 °C to 1100 °C): Hyperfine Field: B_{hf} (T), Quadrupole Splitting: QS (mm/s), Relative Intensity: Rel. Int. (%), Center Shift: CS (mm/s) and the Width of inner line: W (mm/s)

Mössbauer parameter	T = 700°C (A-700)	T = 800°C (A-800)	T = 900°C (A-900)	T = 1000°C (A-1000)	T = 1100°C (A-1100)
χ^2	1.91	4.45	6.63	3.39	6.41
CS I (± 0.01)	0.21	0.11	0.12	0.12	0.12
CS II (± 0.01)	0.09	0.19	0.19	0.19	0.20
CS III (± 0.01)	0.17	0.17	0.17	0.16	0.16
CS IV (± 0.01)	0.12	–	–	–	–
CS (± 0.01) (doublet)	0.14	0.05	0.05	–	–
B_{hf} I (± 0.1)	50.9	46.7	46.6	46.7	47.1
B_{hf} II (± 0.1)	47.8	43.7	43.6	43.7	44.2
B_{hf} III (± 0.1)	41.6	39.5	39.5	39.8	40.3
B_{hf} IV (± 0.1)	39.0	–	–	–	–
QS I (± 0.02)	0.09	–	–	–	–
QS II (± 0.02)	0.10	–	–	–	–
QS III (± 0.02)	0.23	–	–	–	–
QS IV (± 0.02)	0.06	–	–	–	–
QS (doublet) (± 0.02)	0.72	0.84	1.08	–	–
Rel. Int. (I) (± 1)	7	24	23	25	25
Rel. Int. (II) (± 1)	51	48	49	50	50
Rel. Int. (III) (± 1)	19	24	25	25	25
Rel. Int. (IV) (± 1)	13	–	–	–	–
Rel. Int. (doublet) (± 1)	10	4	3	–	–
W(I) (± 0.02)	0.21	0.33	0.31	0.31	0.31
W(II) (± 0.02)	0.45	0.48	0.47	0.48	0.48
W(III) (± 0.02)	0.40	0.50	0.51	0.51	0.49
W(IV) (± 0.02)	0.63	–	–	–	–
W(doublet) (± 0.02)	0.47	0.59	0.72	–	–

obtained by others [48, 49]. The presence of the BaM-type phase in the A-700 sample agrees with the fact that the M-type phase is an intermediate phase in the course of crystallization of the Co_2Y phase [50, 51]. The last component (quadrupole doublet) with $\text{QS} = 0.72$ mm/s and Rel. Int. = 10% is attributed to spinel ferrites species in a superparamagnetic phase which agrees with our XRD results and the results for spinel (CoFe_2O_4 and Fe_3O_4) reported by others [52, 53].

Mössbauer spectra of the samples A-800 and A-900 were each fitted with three magnetic sextet components (I, II, III) and one quadrupole doublet. The first sextet component (I) is associated with the ($6c_{\text{IV}}^* + 3b_{\text{VI}}$) sites, the second sextet component (II) is 2 associated with the $18h_{\text{VI}}$ sites, while the third sextet component (III) is associated with the ($6c_{\text{VI}} + 6c_{\text{IV}} + 3a_{\text{VI}}$) sites. The relative intensities of these components are in excellent agreement with the theoretical ratios of 25:50:25, consistent with Co^{2+} ions filling the $6c_{\text{VI}}$ sites. The fourth small (3–4%) doublet component with quadrupole splitting $\text{QS} = 0.84$ mm/s and 1.08 mm/s for the two samples, respectively, is attributed to the nonmagnetic barium spinel phase detected by XRD. The observed values of the quadrupole splitting agree with that reported for Ba-spinel [54].

On the other hand, Mössbauer spectra of the samples A-1000 and A-1100 were each fitted with the three magnetic sextet components (I, II, III) associated with the magnetic sublattices of the Co_2Y structure. The absence of other components in Mössbauer spectra of these samples is a further confirmation that these samples are composed of pure Y-type hexaferrite phase.

- $\text{Ba}_2\text{Co}_2\text{Fe}_{12}\text{O}_{22}$ (B, 700°C to 1100°C) Samples

The Mössbauer spectra for the B-700, B-800, B-900, B-1000 and B-1100 samples are shown in Fig. 6. The figure shows different spectral structure for the different samples, which is significantly different from the spectral shape for the samples prepared by route A. A first look at the spectra with an expert eye indicates that none of the samples consisted of a Y-type hexaferrite phase with relatively high purity. The spectra were fitted with four broad magnetic sextets components and one quadrupole doublet; the fitting hyperfine parameters are listed in Table 4.

The Mössbauer spectrum for the B-700 is fitted with four broad magnetic sextet components and one quadrupole doublet. The values of hyperfine fields were $B_{\text{hf}} = 49.3$ T, 47.6 T, 43.3 T and 39.4 T and the doublet quadrupole splitting $QS = 0.62$ mm/s. The first two

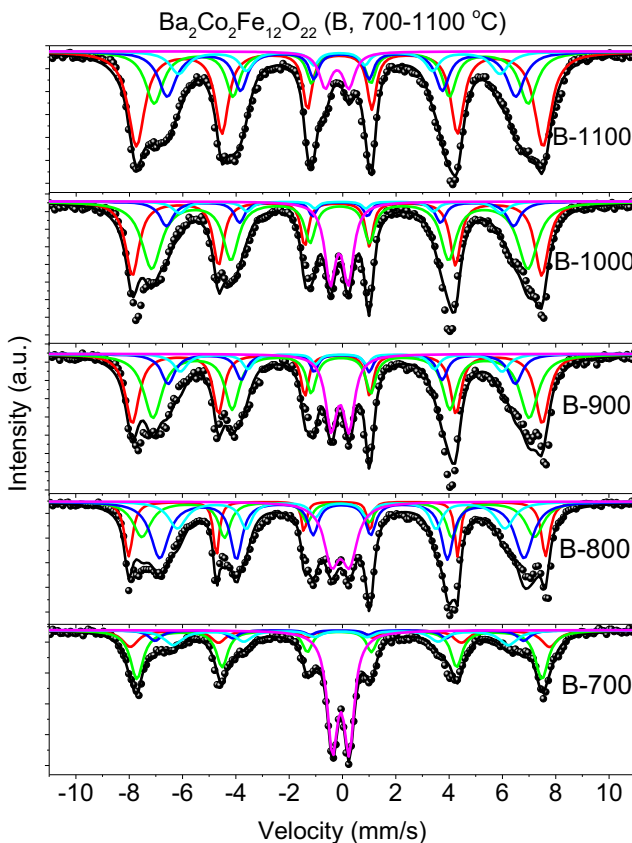


Fig. 6 Mössbauer spectra for the $\text{Ba}_2\text{Co}_2\text{Fe}_{12}\text{O}_{22}$ samples (B-700, B-800, B-900, B-1000 and B-1100) prepared using procedure B and sintered at different temperatures (700 °C to 1100 °C)

Table 4 Mössbauer parameters of the spectral component for samples prepared by procedure B and sintered at different temperatures: Hyperfine Field: B_{hf} (T), Quadrupole Splitting: QS (mm/s), Relative Intensity (%), Center Shift: CS (mm/s) and the Width (mm/s)

Mössbauer parameter	T = 700°C (B-700)	T = 800°C (B-800)	T = 900°C (B-900)	T = 1000°C (B-1000)	T = 1100°C (B-1100)
χ^2	1.59	9.31	4.49	7.17	3.24
CS I (± 0.01)	0.10	-0.09	-0.08	0.09	0.01
CS II (± 0.01)	0.00	-0.05	0.06	0.01	0.05
CS III (± 0.01)	-0.01	0.09	0.09	0.02	0.06
CS IV (± 0.01)	0.05	0.06	0.07	0.03	0.03
CS (± 0.01)	0.05	0.04	0.04	0.01	0.10
Doublet					
B_{hf} I (± 0.1)	49.3	49.0	48.2	48.1	48.0
B_{hf} II (± 0.1)	47.6	46.1	44.2	44.2	44.2
B_{hf} III (± 0.1)	43.3	42.8	40.8	40.8	40.8
B_{hf} IV (± 0.1)	39.4	38.5	37.8	37.8	37.4
QS (doublet) (± 0.02)	0.62	0.67	0.67	0.67	0.90
Rel. Int. I (± 1)	14	15	30	31	31
Rel. Int. II (± 1)	34	21	37	41	40
Rel. Int. III (± 1)	7	34	13	10	16
Rel. Int. IV (± 1)	14	16	8	5	8
Rel. Int. (± 1) (doublet)	31	14	12	13	5
W(I) (± 0.02)	0.55	0.22	0.35	0.35	0.37
W(II) (± 0.02)	0.45	0.47	0.46	0.50	0.56
W(III) (± 0.02)	0.42	0.47	0.34	0.35	0.37
W(IV) (± 0.02)	0.62	0.47	0.34	0.35	0.37
W(± 0.02) (doublet)	0.47	0.70	0.50	0.48	0.54

components with $B_{\text{hf}} = 49.3$ T and 47.6 T has relative intensities of 14% and 34%, which is close enough to the ratio of 1:2 for the number of Fe ions at tetrahedral and octahedral sites of the cubic spinel structure of magnetite (Fe_3O_4). The hyperfine field values and relative intensities of these two components may be an indication of the presence of magnetite phase in this sample. Similarly, the two components with $B_{\text{hf}} = 43.3$ and 39.4 T could be associated with Co-spinel (CoFe_2O_4) ferrite phase. The hyperfine fields for these components are in general agreement with the range of hyperfine fields reported for cubic spinel ferrites [46, 52]. The quadrupole doublet with QS = 0.62 mm/s is attributed to Ba-spinel (BaFe_2O_4) phase. The phases associated with the different Mössbauer components were confirmed by the XRD patterns for this sample (B-700).

The four magnetic components in Mössbauer spectra for the rest of the samples (B-800 to B-1100) are associated with the superposition of the spectra of cubic spinel, and Co_2Y phases. Specifically, the hyperfine field for the first component (~ 48 –49 T) is in agreement with that for the high-field component in the spinel structure. The other component of the spinel phase, however, could be buried under the components of the Y-type phase due to similar hyperfine field. The quadrupole doublet in the spectra of the samples B-800 to B-1000 (QS = 0.67 mm/s) could be associated with the barium spinel phase, whereas the quadrupole doublet with QS = 0.9 mm/s for the sample B-1100 could be associated with superparamagnetic particles as discussed before.

4 Conclusion

This work reported the results of structural and Mössbauer spectroscopy for $\text{Ba}_2\text{Co}_2\text{Fe}_{12}\text{O}_{22}$ samples prepared by coprecipitation method with variations in the experimental conditions. The results of this study indicated that the dropwise addition of the precipitation agent to achieve $\text{pH} = 10$ resulted in the crystallization of the Y-type hexagonal phase with high purity at temperatures as low as 800°C . On the contrast, such a high purity Y-type hexagonal phase could not be achieved by route B where the pH is higher ($\text{pH} = 14$) and the addition of the precipitation agent is a quick one (one shot). The average crystallite size for the Y-type hexagonal phase (prepared with $\text{pH} = 10$) is found to grow monotonically from 65 nm to 86 nm with sintering temperature, while the average value stays around 50 nm for the Y-phase resulted by route B ($\text{pH} = 14$). Future work will include variation of type of precipitant, the method of addition and the pH value on the quality and purity of hexaferrite phase.

Acknowledgements The authors acknowledge the contribution of Prof. I. Bsoul at Al al-Bayt University in the Rietveld refinement analysis. The Financial support of the Deanship of Scientific Research and Graduate Studies at Yarmouk University is acknowledged. A-F. Lehlooh appreciates the full support of Yarmouk University to attend ICAME 2019 in Dalian.

References

1. Smit, J., Wijn, H.P.J.: Ferrites. Wiley, New York (1959)
2. Chikazumi, S.: Physics of Ferromagnetism 2e, 2nd edn. Oxford University Press, Oxford (2009)
3. Pullar, R.C.: Hexagonal ferrites: a review of the synthesis, properties and applications of hexaferrite ceramics. *Prog. Mater. Sci.* **57**, 1191–1334 (2012)
4. Harris, V.G., Geiler, A., Chen, Y., Yoon, S.D., Wu, M., Yang, A., Chen, Z., He, P., Parimi, P.V., Zuo, X.: Recent advances in processing and applications of microwave ferrites. *J. Magn. Mater.* **321**, 2035–2047 (2009)
5. Özgür, Ü., Alivov, Y., Morkoç, H.: Microwave ferrites, part 1: fundamental properties. *J. Mater. Sci. Mater. Electron.* **20**, 789–834 (2009)
6. Mahmood, S.H.: Permanent magnet applications. In: Mahmood, S.H., Abu-Aljarayesh, I. (eds.) Hexaferrite Permanent Magnetic Materials, pp. 153–165. Materials Research Forum LLC, Millersville (2016)
7. Nicolas, J.: Microwave ferrites. In: Wohlfarth, E.P. (ed.) Ferromagnetic Materials, pp. 243–296. North-Holland Publishing Company, New York (1980)
8. Topal, U., Bakan, H.I.: Permanently magnetic $\text{BaFe}_{12}\text{O}_{19}$ foams: synthesis and characterization. *Mater. Chem. Phys.* **123**, 121–124 (2010)
9. Hongya, Y., Zhengyi, L., Dechang, Z.: Microstructure of pre-sintered permanent magnetic strontium ferrite powder. *Rare Metals.* **25**, 572–577 (2006)
10. Kubo, O., Ido, T., Yokoyama, H.: Properties of Ba ferrite particles for perpendicular magnetic recording media. *IEEE Trans. Magn.* **18**, 1122–1124 (1982)
11. Speliotis, D.: Barium ferrite magnetic recording media. *IEEE Trans. Magn.* **23**, 25–28 (1987)
12. Taniguchi, K., Abe, N., Ohtani, S., Umetsu, H., Arima, T.-h.: Ferroelectric polarization reversal by a magnetic field in multiferroic Y-type hexaferrite $\text{Ba}_2\text{Mg}_2\text{Fe}_{12}\text{O}_{22}$. *Appl. Phys. Express.* **1**, 031301 (2008)
13. Lee, H.B., Chun, S.H., Shin, K.W., Jeon, B.-G., Chai, Y.S., Kim, K.H., Schefer, J., Chang, H., Yun, S.-N., Joung, T.-Y.: Helical magnetic order and field-induced multiferroicity of the Co_2Y -type hexaferrite $\text{Ba}_{0.3}\text{Sr}_{1.7}\text{Co}_2\text{Fe}_{12}\text{O}_{22}$. *Phys. Rev. B.* **86**, 094435 (2012)
14. Tokura, Y., Seki, S.: Multiferroics with spiral spin orders. *Adv. Mater.* **22**, 1554–1565 (2010)
15. Tabatabaie, F., Fathi, M., Saatchi, A., Ghasemi, A.: Effect of Mn-co and co-Ti substituted ions on doped strontium ferrites microwave absorption. *J. Alloys Compd.* **474**, 206–209 (2009)
16. Sharma, S., Daya, K., Sharma, S., Batoo, K.M., Singh, M.: Sol-gel auto combustion processed soft Z-type hexa nanoferrites for microwave antenna miniaturization. *Ceram. Int.* **41**, 7109–7114 (2015)
17. Geiler, A., Daigle, A., Wang, J., Chen, Y., Vittoria, C., Harris, V.: Consequences of magnetic anisotropy in realizing practical microwave hexaferrite devices. *J. Magn. Mater.* **324**, 3393–3397 (2012)

18. Mahmood, S.H.: Ferrites with high magnetic parameters. In: Mahmood, S.H., Abu-Aljarayesh, I. (eds.) *Hexaferrite Permanent Magnetic Materials*, pp. 111–152. Materials Research Forum LLC, Millersville (2016)
19. Mahmood, S.H., Bsoul, I.: Tuning the magnetic properties of M-type hexaferrites. In: Jotania, R.B., Mahmood, S.H. (eds.) *Magnetic Oxides and Composites*, pp. 49–100. Materials Research Forum LLC, Millersville (2018)
20. Topal, U.: A simple synthesis route for high quality $\text{BaFe}_{12}\text{O}_{19}$ magnets. *Mater. Sci. Eng. B.* **176**, 1531–1536 (2011)
21. Topal, U.: Towards further improvements of the magnetization parameters of B_2O_3 -doped $\text{BaFe}_{12}\text{O}_{19}$ particles: etching with hydrochloric acid. *J. Supercond. Nov. Magn.* **25**, 1485–1488 (2012)
22. Sözeri, H., Durmuş, Z., Baykal, A., Uysal, E.: Preparation of high quality, single domain $\text{BaFe}_{12}\text{O}_{19}$ particles by the citrate sol-gel combustion route with an initial Fe/Ba molar ratio of 4. *Mater. Sci. Eng. B.* **177**, 949–955 (2012)
23. Han, M., Ou, Y., Chen, W., Deng, L.: Magnetic properties of Ba-M-type hexagonal ferrites prepared by the sol-gel method with and without polyethylene glycol added. *J. Alloys Compd.* **474**, 185–189 (2009)
24. Dursun, S., Topkaya, R., Akdoğan, N., Alkoy, S.: Comparison of the structural and magnetic properties of submicron barium hexaferrite powders prepared by molten salt and solid state calcination routes. *Ceram. Int.* **38**, 3801–3806 (2012)
25. Kim, D.-H., Lee, Y.-K., Kim, K.-M., Kim, K.-N., Choi, S.-Y., Shim, I.-B.: Synthesis of Ba-ferrite microspheres doped with Sr for thermoseeds in hyperthermia. *J. Mater. Sci.* **39**, 6847–6850 (2004)
26. Pullar, R., Bhattacharya, A.: The magnetic properties of aligned M hexa-ferrite fibres. *J. Magn. Magn. Mater.* **300**, 490–499 (2006)
27. Alsmadi, A., Bsoul, I., Mahmood, S., Alnawashi, G., Al-Dweri, F., Maswadeh, Y., Welp, U.: Magnetic study of M-type Ru-Ti doped strontium hexaferrite nanocrystalline particles. *J. Alloys Compd.* **648**, 419–427 (2015)
28. Palomino, R., Miró, A.B., Tenorio, F., De Jesús, F.S., Escobedo, C.C., Ammar, S.: Sonochemical assisted synthesis of $\text{SrFe}_{12}\text{O}_{19}$ nanoparticles. *Ultrason. Sonochem.* **29**, 470–475 (2016)
29. Singhal, S., Namgyal, T., Singh, J., Chandra, K., Bansal, S.: A comparative study on the magnetic properties of $\text{MFe}_{12}\text{O}_{19}$ and $\text{MAlFe}_{11}\text{O}_{19}$ (M= Sr, Ba and Pb) hexaferrites with different morphologies. *Ceram. Int.* **37**, 1833–1837 (2011)
30. Guerrero-Serrano, A., Pérez-Juache, T., Mirabal-García, M., Matutes-Aquino, J., Palomares-Sánchez, S.: Effect of barium on the properties of lead hexaferrite. *J. Supercond. Nov. Magn.* **24**, 2307–2312 (2011)
31. Mahmood, S.H., Zaqasaw, M.D., Mohsen, O.E., Awadallah, A., Bsoul, I., Awawdeh, M., Mohaidat, Q.I.: Modification of the magnetic properties of Co_2Y hexaferrites by divalent and trivalent metal substitutions. *Solid State Phenom.* **241**, 93–125 (2016)
32. Ali, I., Islam, M., Awan, M., Ahmad, M.: Effects of Ga-Cr substitution on structural and magnetic properties of hexaferrite ($\text{BaFe}_{12}\text{O}_{19}$) synthesized by sol-gel auto-combustion route. *J. Alloys Compd.* **547**, 118–125 (2013)
33. Awawdeh, M., Al-Bashaireh, R., Lehlooh, A., Mahmood, S.: Structural and Mossbauer studies of ball milled Co-Zn Y-type hexaferrites. *Jordan J. Phys.* **7**, 85–98 (2014)
34. Dahal, J., Wang, L., Mishra, S., Nguyen, V., Liu, J.: Synthesis and magnetic properties of $\text{SrFe}_{12-x-y}\text{Al}_y\text{Co}_y\text{O}_{19}$ nanocomposites prepared via autocombustion technique. *J. Alloys Compd.* **595**, 213–220 (2014)
35. Kazin, P., Trusov, L., Zaitsev, D., Tretyakov, Y.D., Jansen, M.: Formation of submicron-sized $\text{SrFe}_{12-x}\text{Al}_x\text{O}_{19}$ with very high coercivity. *J. Magn. Magn. Mater.* **320**, 1068–1072 (2008)
36. Mahmood, S.H., Jaradat, F.S., Lehlooh, A.F., Hammoudeh, A.: Structural properties and hyperfine interactions in co-Zn Y-type hexaferrites prepared by sol-gel method. *Ceram. Int.* **40**, 5231–5236 (2014)
37. Albanese, G., Deriu, A.: Magnetic properties of Al, Ga, Sc, In substituted barium ferrites: a comparative analysis. *Ceram. Int.* **5**, 3–10 (1979)
38. Mazumdar, S.C., Hossain, A.A.: Synthesis and magnetic properties of $\text{Ba}_2\text{Ni}_{2-x}\text{Zn}_x\text{Fe}_{12}\text{O}_{22}$. *World J. Condens. Matter. Phys.* **2**, 181–187 (2012)
39. Bai, Y., Zhou, J., Gui, Z., Li, L.: Magnetic properties of Cu, Zn-modified Co_2Y hexaferrites. *J. Magn. Magn. Mater.* **246**, 140–144 (2002)
40. Albanese, G.: Recent advances in hexagonal ferrites by the use of nuclear spectroscopic methods. *Le Journal de Physique Colloques.* **38**, 85–94 (1977)
41. Khanduri, H., Dimri, M.C., Kooskora, H., Heinmaa, I., Viola, G., Ning, H., Reece, M., Krustok, J., Stern, R.: Structural, dielectric, magnetic, and nuclear magnetic resonance studies of multiferroic Y-type hexaferrites. *J. Appl. Phys.* **112**, 073903 (2012)
42. Sagayama, H., Taniguchi, K., Abe, N., Arima, T.-h., Nishikawa, Y., Yano, S.-i., Kousaka, Y., Akimitsu, J., Matsuura, M., Hirota, K.: Two distinct ferroelectric phases in the multiferroic Y-type hexaferrite $\text{Ba}_2\text{Mg}_2\text{Fe}_{12}\text{O}_{22}$. *Phys. Rev. B.* **80**, 180419 (2009)

43. Bai, Y., Zhou, J., Gui, Z., Yue, Z., Li, L.: Preparation and magnetic characterization of Y-type hexaferrites containing zinc, cobalt and copper. *Mater. Sci. Eng. B.* **99**, 266–269 (2003)
44. Collins, E.D, Voit, S.L, and Vedder, R.J.: Evaluation of Co-precipitation Processes for the Synthesis of Mixed-Oxide Fuel Feedstock Materials. United States: N. p., 2011. <https://doi.org/10.2172/1024695>.
45. Hsiang, H.-I., Yao, R.-Q.: Hexagonal ferrite powder synthesis using chemical coprecipitation. *Mater. Chem. Phys.* **104**, 1–4 (2007)
46. Aneesh Kumar, K.S., Bhowmik, R.N., Mahmood, S.H.: Role of pH value durinh chemical reaction, and site occupancy of Ni²⁺ and Fe³⁺ ions in spinel structure for tuning room temperature magnetic properties in Ni_{1.5}Fe_{1.5}O₄ ferrite. *J. Magn. Magn. Mater.* **406**, 60–71 (2016)
47. Warren, B.E.: X-Ray Diffraction. Addison-Wesley, Reading (1969)
48. Evans, B., Grandjean, F., Lilot, A., Vogel, R., Gerard, A.: 57Fe hyperfine interaction parameters and selected magnetic properties of high purity MFe₁₂O₁₉ (M= Sr, Ba). *J. Magn. Magn. Mater.* **67**, 123–129 (1987)
49. Awadallah, A., Mahmood, S.H., Maswadeh, Y., Bsoul, I., Awawdeh, M., Mohaidat, Q.I., Juwhari, H.: Structural, magnetic, and Mossbauer spectroscopy of cu substituted M-type hexaferrites. *Mater. Res. Bull.* **74**, 192–201 (2016)
50. Daigle, A., DuPre, E., Geiler, A., Chen, Y., Parimi, P.V., Vittoria, C., Harris, V.G.: Preparation and characterization of pure-phase Co₂Y ferrite powders via a scalable aqueous Coprecipitation method. *J. Am. Ceram. Soc.* **93**, 2994–2997 (2010)
51. Lisjak, D., Drogenik, M.: The low-temperature formation of barium hexaferrites. *J. Eur. Ceram. Soc.* **26**, 3681–3686 (2006)
52. Aphesteguy, J.C., Jacobo, S.E., Schegoleva, N., Kurlyandskaya, G.: Characterization of nanosized spinel ferrite powders synthesized by coprecipitation and autocombustion method. *J. Alloys Compd.* **495**, 509–512 (2010)
53. D. Kovacheva, T. Ruskov, P. Krystev, S. Asenov, N. Tanev, I. Mönch, R. Koseva, U. Wolff, T. Gemming, M. Markova-Velichkova, Synthesis and characterization of magnetic nano-sized Fe₃O₄ and CoFe₂O₄, Bulgarian Chemical Communications Proceedings of the III rd National Crystallographic Symposium, 2012, pp. 90–97
54. Mukasyan, A., Dinka, P.: Novel approaches to solution-combustion synthesis of nanomaterials. *Int. J. Self-Propag. High-Temp. Synth.* **16**, 23–35 (2007)

Publisher's note Springer Nature remains neutral with regard to jurisdictional claims in published maps and institutional affiliations.